Supporting Information

A General Solid-State Synthesis of Chemically-Doped Fluorescent Graphene Quantum Dots for Bioimaging and Optoelectronic Applications

Chong-Bo Ma[a], Zhen-Tong Zhu[a], Hang-Xing Wang[a], Xiao Huang[b], Xiao Zhang[b], Xiaoying Qi[c], Hao-Li Zhang,[a,*] Yihan Zhu[d], Xia Deng[e], Yong Peng[e], Yu Han[d] and Hua Zhang[b,*]

[a]State Key Laboratory of Applied Organic Chemistry (SKLAOC), College of Chemistry and Chemical Engineering Lanzhou University, Lanzhou, 730000 (R. P. China)
[b]School of Materials Science and Engineering, Nanyang Technological University, 50 Nanyang Avenue, Singapore 639798, Singapore.
[c]Singapore Institute of Manufacturing Technology, 71 Nanyang Drive, Singapore 638075, Singapore.
[d]Advanced Membranes and Porous Materials Center, Physical Sciences and Engineering Division, King Abdullah University of Science and Technology, Thuwal 23955-6900, Saudi Arabia
[e]Key Laboratory of Magnetism and Magnetic Materials of Ministry of Education, School of Physical Science and Technology, Lanzhou University, Lanzhou 730000, China

*Corresponding authors. E-mail: Haoli.zhang@lzu.edu.cn; hzhang@ntu.edu.sg;

Table S1. Optimization of reaction conditions for synthesis of E-GQDs.

Reaction condition	Below 240 °C 5 min	240-260 °C 5 min	260-280 °C 5 min	Above 280 °C, 5 min
Product	No reaction	Low yield very small particles (size below 5 nm)	Uniform particles with few sheets	Particles with large sheet structures

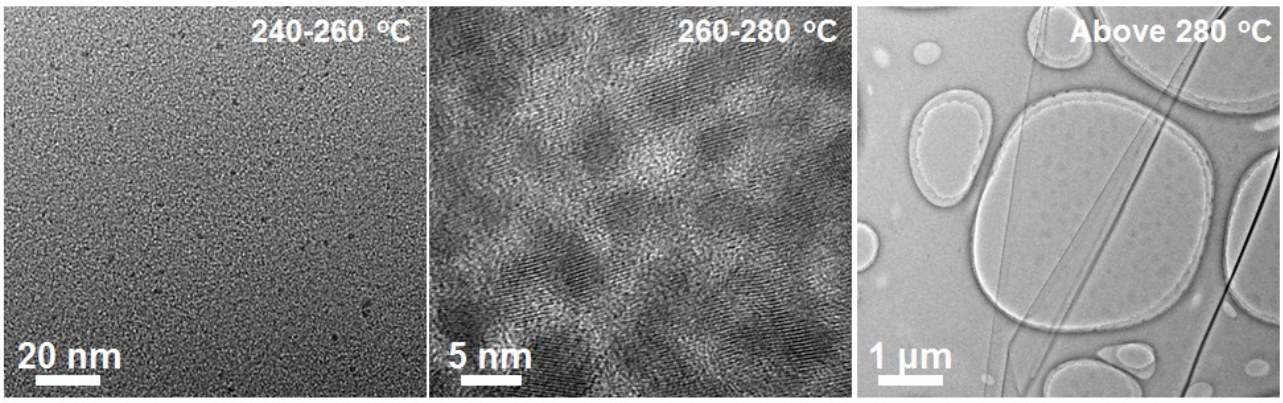

Figure S1. TEM images of products under different reaction conditions.

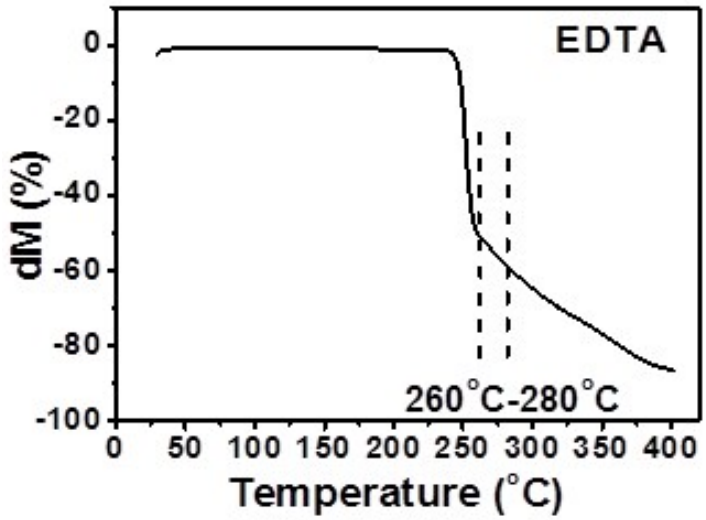

Figure S2. The thermogravimetry analysis (TGA) curve of EDTA giving the optimal reaction temperature range for synthesis of E-GQDs.

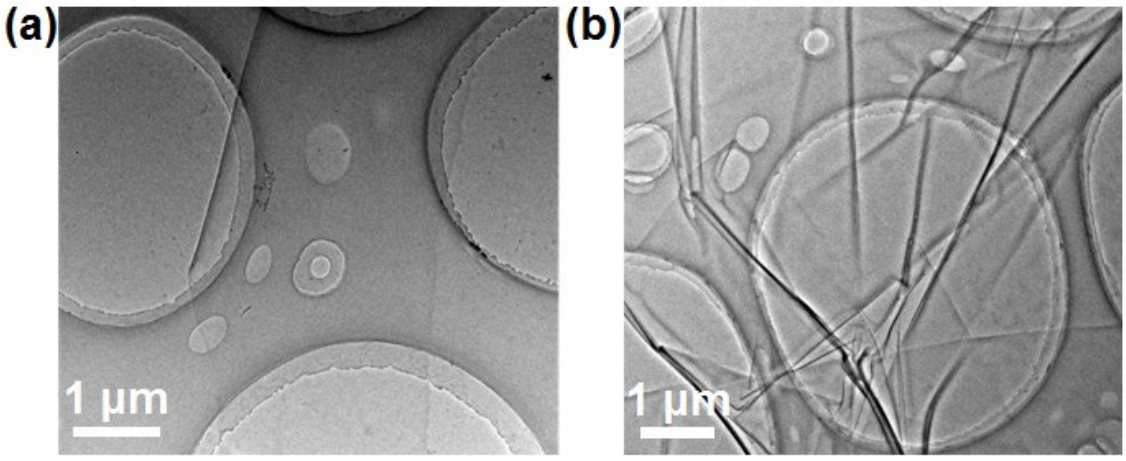

Figure S3. TEM image of microsized flakes obtained at higher reaction temperature (i.e. > 280 ^{o}C) (a) and longer reaction time (e.g. 10 min) (b).

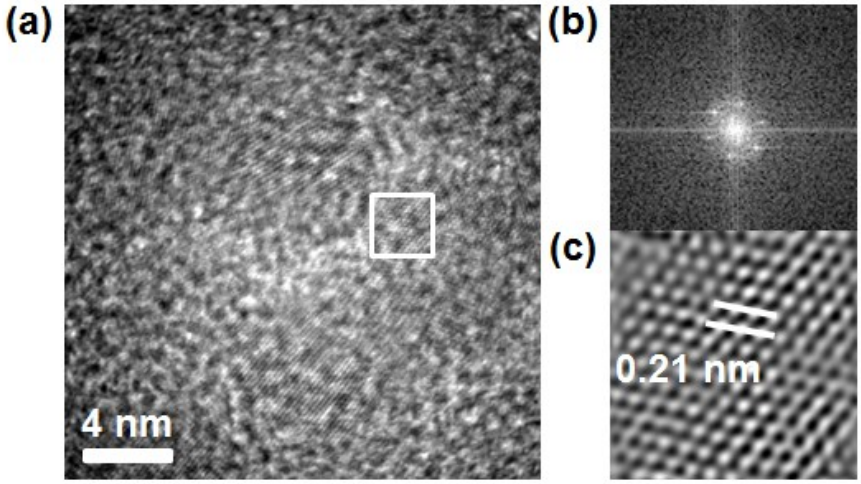

Figure S4. Characterizations of E-GQDs. (a) HRTEM image, (b) the corresponding Fast Fourier Transform (FFT) image of the area shown in the white square in (a), (c) the filtered HRTEM image obtained after deduction of the background signal of amorphous carbon film on Cu grid.

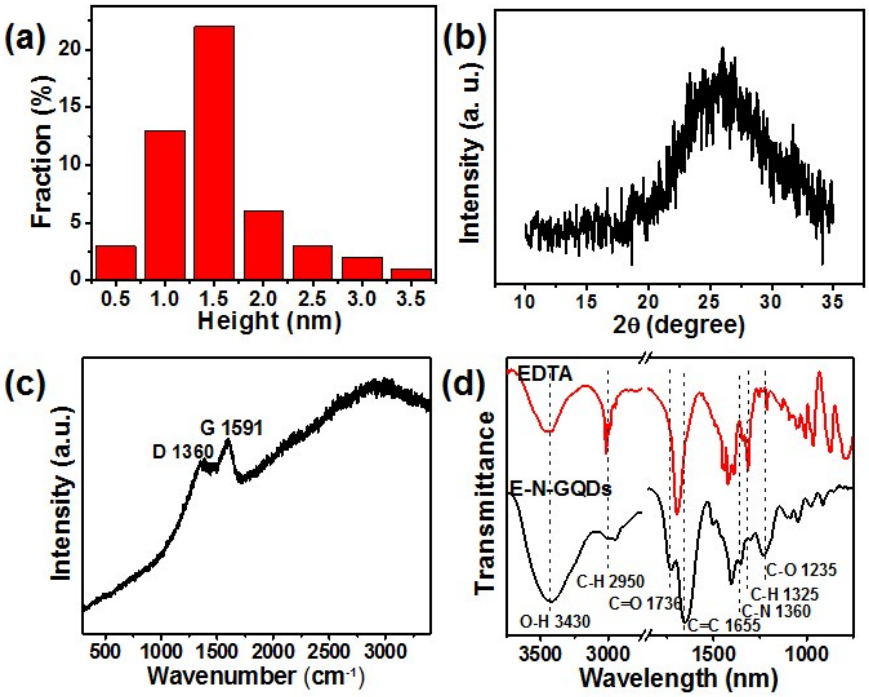

Figure S5. Characterizations of E-GQDs. (a) Height distribution of E-GQDs measured by AFM. (b) XRD pattern of E-GQDs. (c) Raman spectrum of E-GQDs. (d) FT-IR spectra of EDTA and E-GQDs.

Table S2. Carbon (C), oxygen (O) and nitrogen (N) atomic concentrations of the E-GQDs products prepared in the open air (POA) and in oxygen free (POF) atmosphere. The composition data was obtained from XPS.

	C	O	N
POA	44%	42%	14%
POF	49%	36%	15%

The synthesis of POF E-GQDs is described below. 1.5 g EDTA was put in round bottom flask and protected with N_2, and then heated in a sand bath at 260-280 ^oC with vigorous stirring. After cooling down to room temperature, freshly prepared DI water was added to disperse the product. The undissolved residue was removed by centrifugation at 8,000 rpm for 5 min. The supernatant was further purified by centrifugation and filtration using AmiconUltra filter (Millipore, Billerica, MA) with a molecular mass cut-off of 10 kDa to remove large sheets. The final product was collected by dialyzing the aqueous solution with a dialysis membrane bag (MW 1000) for several days to fully remove the residual EDTA.

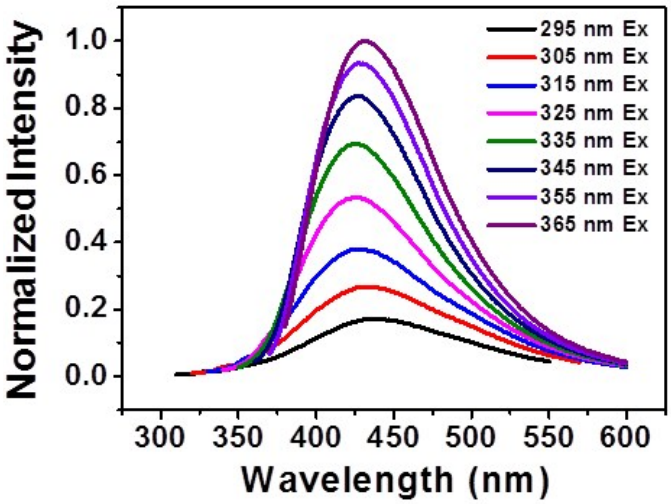

Figure S6. Normalized PL spectra of E-GQDs under the excitation wavelength from 295 to 365 nm.

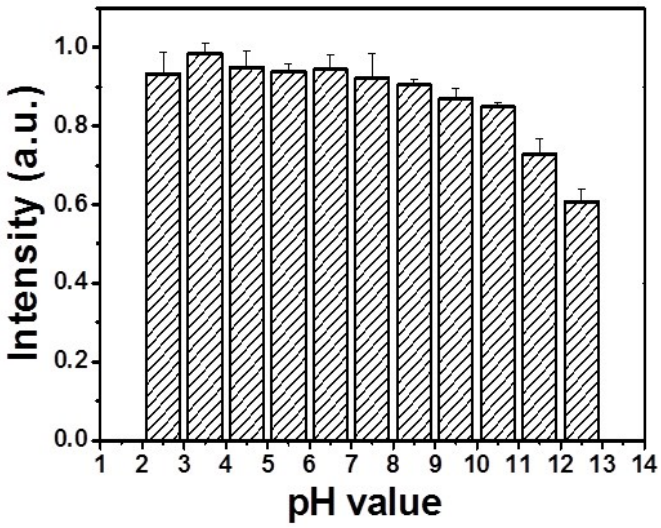

Figure S7. The effect of pH value on the PL intensity of E-GQDs.

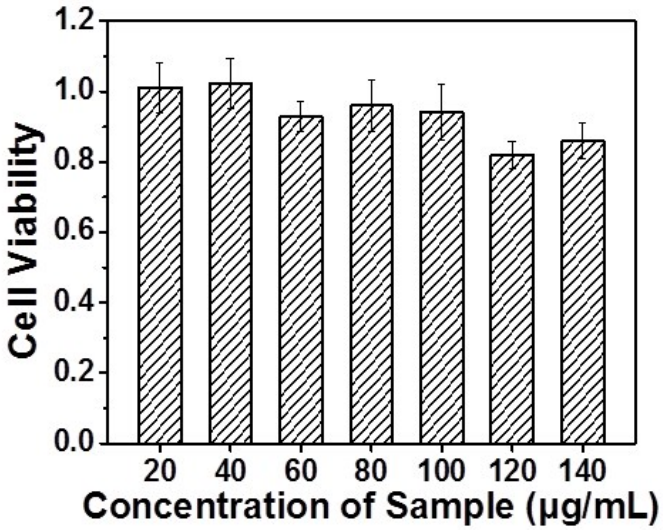

Figure S8. The cell viability using RAW 264.7 cells treated with different concentrations of E-GQD by CCK-8 assay.

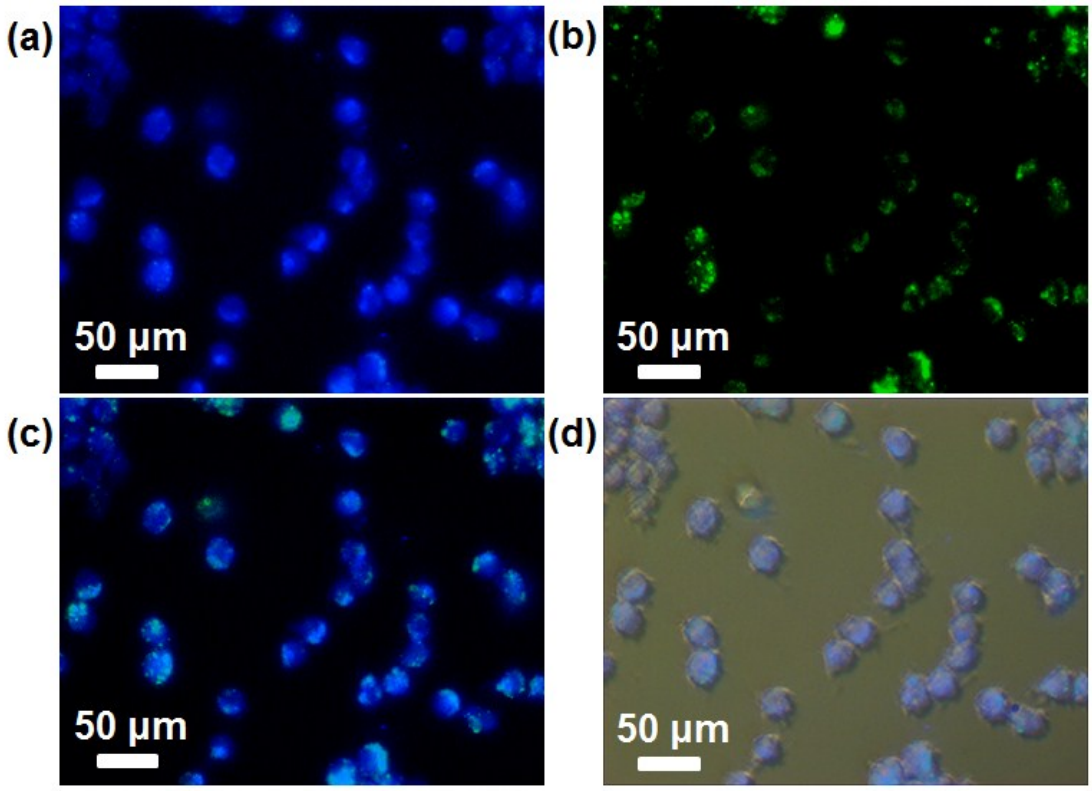

Figure S9. The RAW 264.7 cells were incubated with 80 μg/mL of E-GQDs in PBS (pH 7.4) for 1 h at 37 °C and 5 % CO_2. Then, the cells were lysosome-stained with LysoTracker@Green for 10 min. (a) Fluorescence image of E-GQDs. (b) Fluorescence images of lysosome-staining. (c) Overlay of

the corresponding fluorescence images of (a) and (b). (d) Overlay of the fluorescence image in (a) and its corresponding bright-field image.

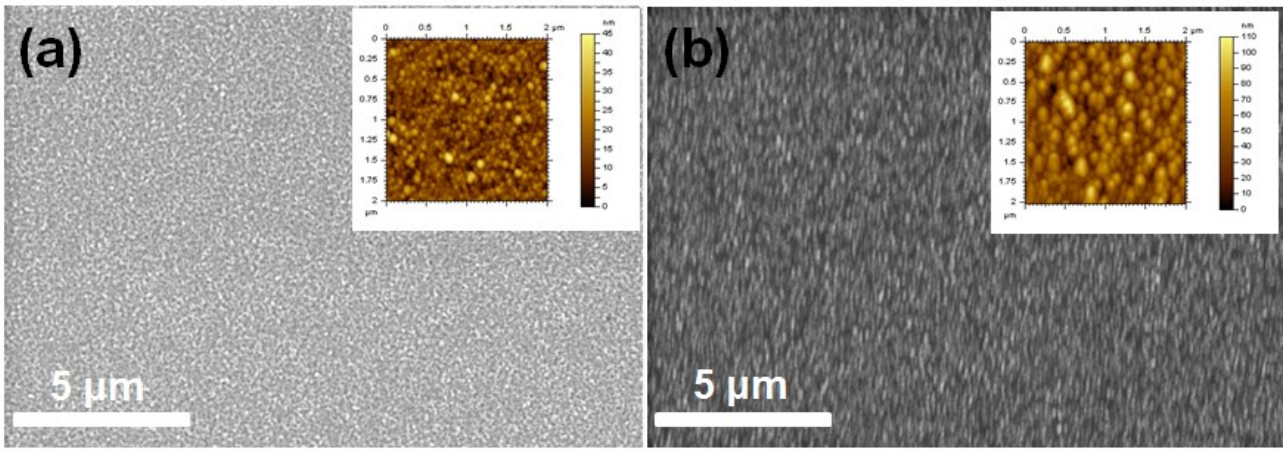

Figure S10. Characterization for thin-films formed by electrophoretic deposition. SEM images of (a) E-GQDs and (b) CA-CDs. Insets: the corresponding AFM images of the films.

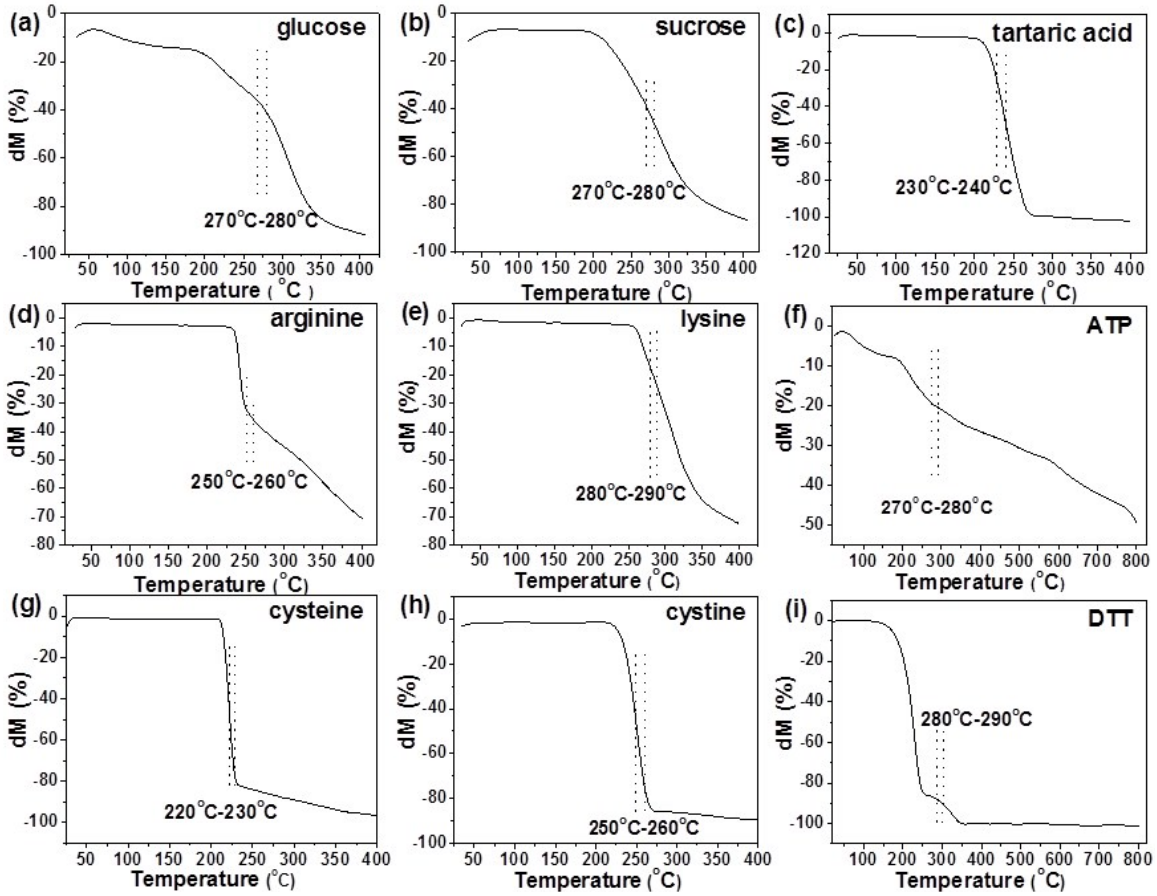

Figure S11. TGA curves of different precursors. The temperature between the dash lines showed the optimal ranges of reaction temperature for synthesis of different GQDs.

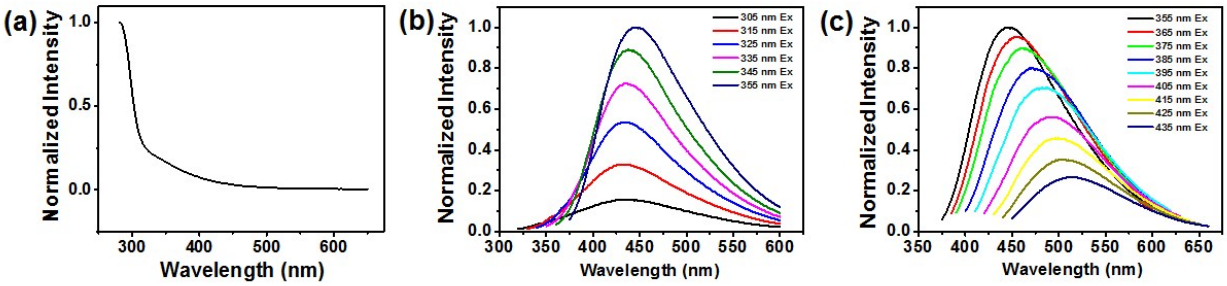

Figure S12. (a) UV-vis absorption spectrum of G-GQDs. The PL spectra of G-GQDs when excited at different wavelength ranging from 305 to 355 nm (b), and from 355 nm to 435 nm (c).

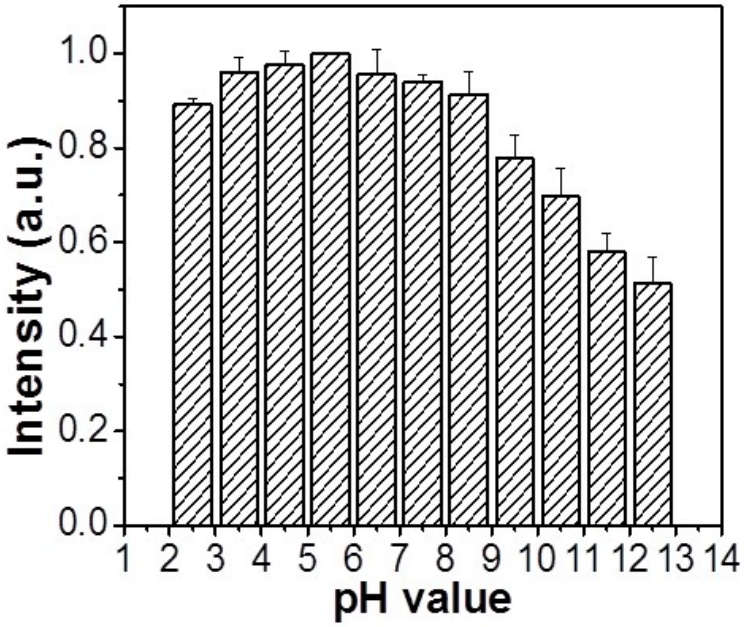

Figure S13. The effect of pH value on the PL intensity of G-GQDs.

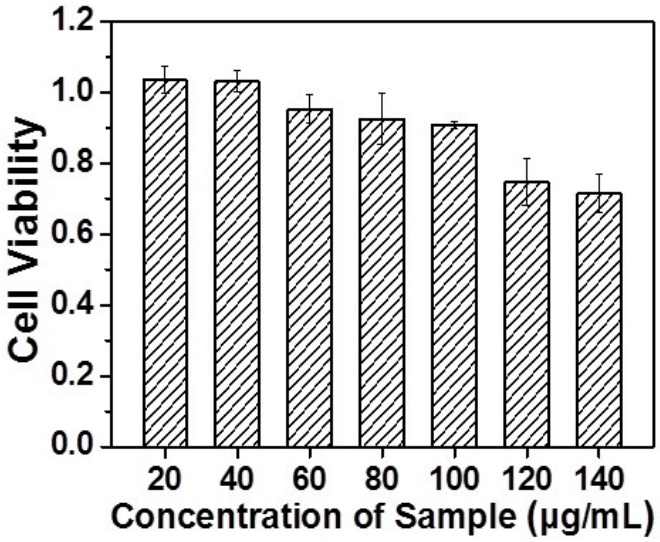

Figure S14. The cell viability with RAW 264.7 cells treated with different concentration of G-GQDs by CCK-8 assay.

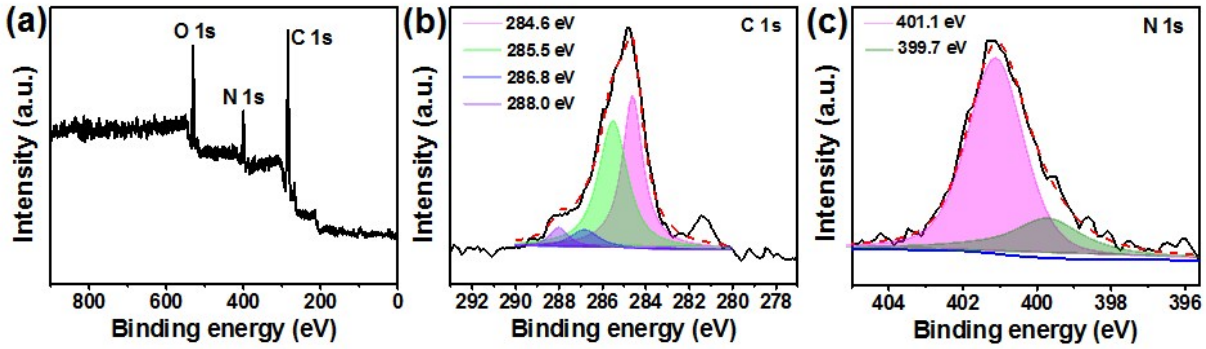

Figure S15. (a) XPS survey spectrum and high-resolution C 1s (b) and N 1s (c) spectra of GQDs synthesized from lysine. The deconvoluted C 1s peaks consists of mainly four individual peaks assignable to C–C (~284.6 eV),[S1a] C–N (~285.5 eV),[S1b] C–O (~286.8 eV),[S1c] and C=O (~288.0 eV) bonds.[S1d] The deconvolution of the N 1s spectrum indicates that N atoms mainly exist as pyrrolic N (~399.7 eV) and quaternary N (~401.1 eV).[S1e]

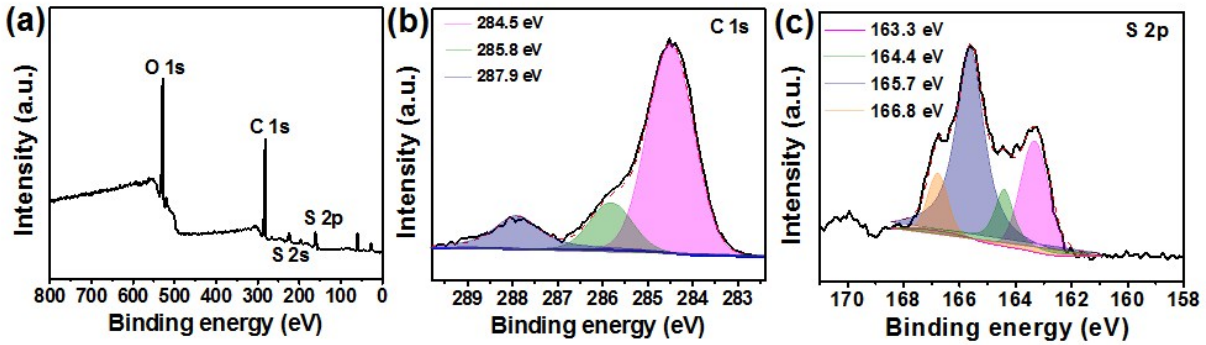

Figure S16. (a) XPS survey spectrum and high-resolution C 1s (b) and S 2p (c) spectra of GQDs synthesized from DTT. The deconvoluted C 1s peaks consists of mainly three individual peaks assignable to sp^2-hybridized C–C (~284.5 eV),[S2a] C–N, C–O, C-S (~285.8 eV)[S2b, c] and C=O (~287.9 eV) bonds.[S2d] The deconvolution of the S 2p spectrum shows the evidence for presence of C-S-C (~163.3 eV and ~164.4 eV), sulfoxides (~165.7 eV) and other oxidized sulfur bond (~166.8 eV).[S2e]

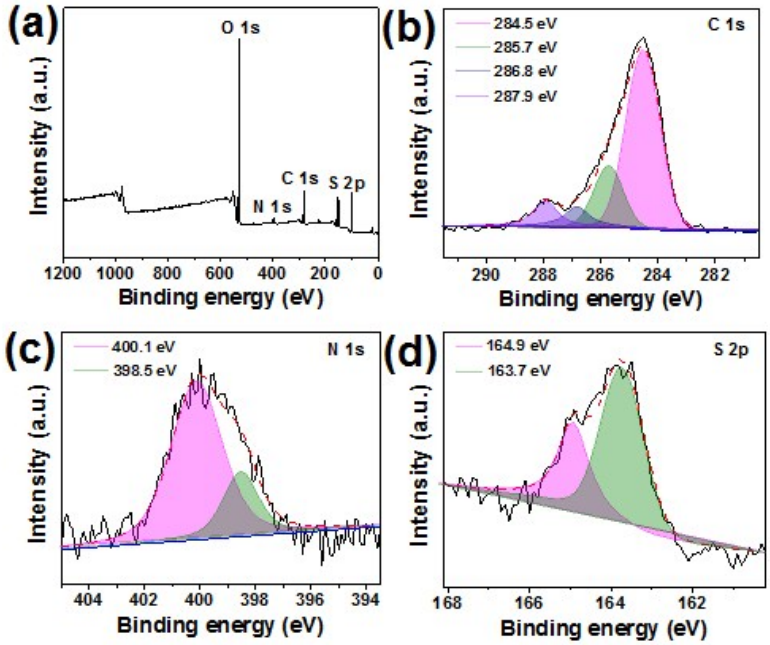

Figure S17. (a) XPS survey spectrum and high-resolution C 1s (b), N 1s (c) and S 2p (d) spectra of GQDs synthesized from cysteine. The deconvoluted C 1s peaks consists of mainly four individual peaks assignable to C–C (~284.5 eV),[S2a] C–N (~285.7 eV),[S3a] C–O (~286.8 eV)[S1c] and C=O (~287.9 eV) bonds.[S2d] The deconvolution of the N 1s spectrum indicates that N atoms mainly exist as pyridine-like sp^2-hybridized form (~398.5 eV) and pyrrole-like sp^3-hybridized form (~400.1 eV).[S3b] The deconvolution of the S 2p spectrum shows the evidence for presence of C-S-C (~163.7 eV and ~164.9 eV).[S3c]

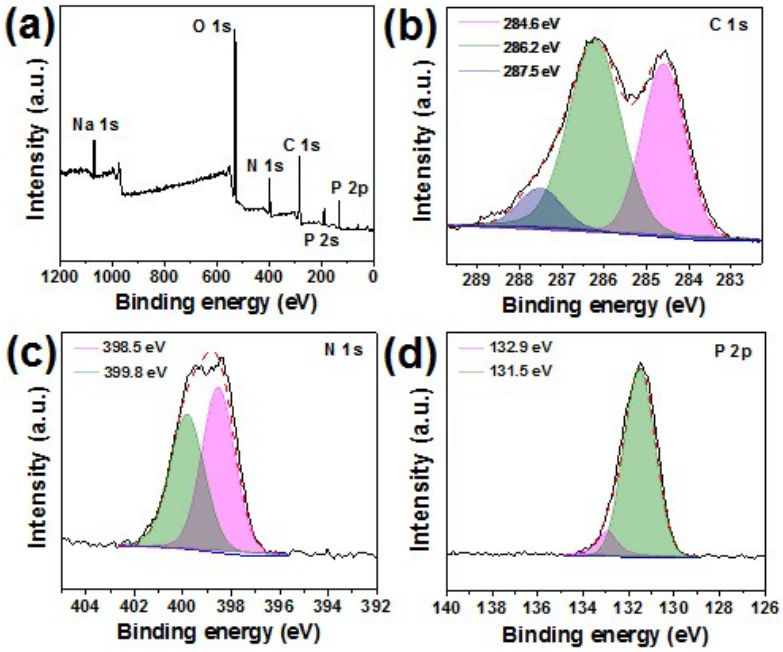

Figure S18. (a) XPS survey spectrum and high-resolution C 1s (b), N 1s (c) and P 2p (d) spectra of GQDs synthesized from ATP. The deconvoluted C 1s peaks consists of mainly four individual peaks assignable to C–C (~284.6 eV),[S1a] C–O, C-N and C=N (~286.2 eV),[S4a] and C=O (~287.5 eV) bonds.[S4b] The deconvolution of the N 1s spectrum indicates that N atoms mainly exist as pyridine-like sp^2-hybridized form (~398.5 eV) and pyrrole-like sp^3-hybridized form (~399.8 eV).[S4c] The deconvolution of the P 2p spectrum indicates that The P atoms are bonded to O atoms (~132.9 eV) and C atoms (~131.5 eV).[S4d]

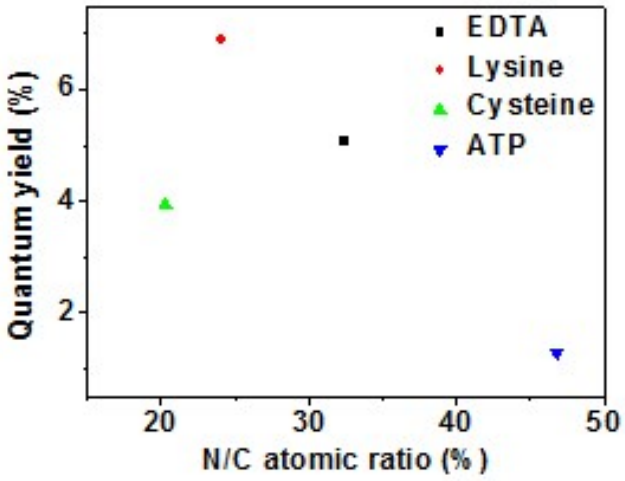

Figure S19. The dependence of fluorescence quantum yield for products from EDTA, lysine, cysteine and ATP on the N/C atomic ratio.

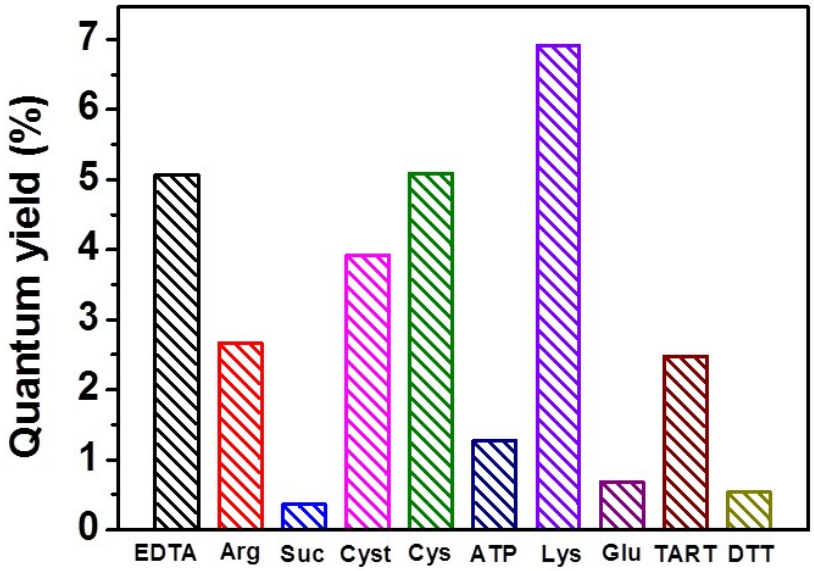

Figure S20. Photoluminescence quantum yields (PLQYs) of products based on the precursors, including EDTA, arginine (Arg), sucrose (Suc), cysteine (Cyst), cysteine (Cys), ATP, lysine (Lys), glucose (Glu), tartaric acid (TART) and DTT.

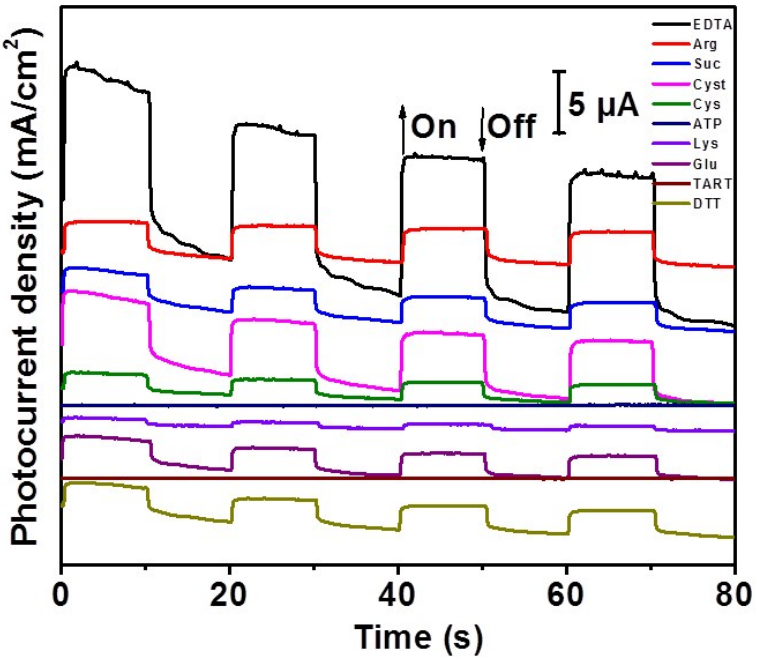

Figure S21. Photocurrent response of products from different precursors, including EDTA, Arg, Suc, Cyst, Cys, ATP, Lys, Glu, TART and DTT.

Table S3. Doping concentrations (DC), referred to as atom percent (atom%), of the doped carbondots based on different precursors (PRO) from XPS quantitative analysis.

PRO / DC / Atom	EDTA	Lysine	DTT	Cysteine	ATP
C	44.1%	55.5%	36.3%	15.5%	24.8%
O	41.6%	31.1%	55.0%	67.6%	56.4%
N	14.3%	13.4%	--	3.14%	11.6%
P	--	--	--	--	7.14%
S	--	--	8.72%	13.8%	--

References

[S1] (a) E. Cano, C. L. Torres and J. M. Bastidas, *Mater. Corros.,* 2001, **52**, 667-676; (b) B. Bouchet-Fabre, K. Zellama, C. Godet, D. Ballutaud and T. Minéa, *Thin Solid Films,* 2005, **482**, 156-166; (c) Y. Li, Y. Zhao, H. Cheng, Y. Hu, G. Shi, L. Dai and L. Qu, *J. Am. Chem. Soc.,* 2012, **134**, 15-18; (d) K. Aumaille, C. Vallée, A. Granier, A. Goullet, F. Gaboriau, G. Turban, *Thin Solid Films,* 2000*,* **359***,* 188-196; (e) D. Jiang, Y. Zhang, H. Chu, J. Liu, J. Wan and M. Chen, *RSC Adv.,* 2014*,* **4***,* 16163–16171.

[S2] (a) D. Joung, A. Chunder, L. Zhai and S. I. Khondaker, *Nanotechnology,* 2010, **21**, 165202; (b) Q. Ding, X. Song, X. Yao, X. Qi, C.-T. Au, W. Zhong and Y. Du, *Nanoscale Res. Lett.,* 2013*,* **8***,* 545; (c) O. Ivashenko, H. Logtenberg, J. Areephong, A. C. Coleman, P. V. Wesenhagen, E. M. Geertsema, N. Heureux, B. L. Feringa, P. Rudolf and W. R. Browne, *J. Phys. Chem. C.,* 2011, **115**, 22965-22975; (d) H. Huang, J. Huang, Y.-M. Liu, H.-Y. He, Y. Cao and K.-N. Fan, *Green Chem.,*

2012, **14**, 930-934; (e) A. Samide, B. Tutunaru, C. Negrila, I. Trandafir and A. Maxut, *Dig. J. Nanomater. Bios.,* 2011, **6**, 663-673.

[S3] (a) K. Zhang, L. Mao, L. L. Zhang, H. S. O. Chan, X. S. Zhao and J. Wu, *J. Mater. Chem.,* 2011, **21**, 7302-7307; (b) R. Arrigo, M. Hävecker, R. Schlögl and D. S. Su, *Chem. Commun.,* 2008, 4891-4893; (c) X. Qing, J. Shi, C. Ma, M. Fan, Z. Bai, Z. Chen, J. Qiao and J. Zhang, *J. Power Sources,* 2014, **266**, 88-98.

[S4] (a) Y. Kusano, T. L. Andersen and P. K. Michelsen, *J. Phys. Conference Series,* 2008, **100**, 012002; (b) Y.-L. Huang, H.-W. Tien, C.-C. M. Ma, S.-Y. Yang, S.-Y. Wu, H.-Y. Liu and Y.-W. Mai, *J. Mater. Chem.,* 2011, **21**, 18236-18241; (c) W. Wang, S. Chakrabarti, Z. Chen, Z. Yan, M. O. Tade, J. Zou and Q. Li, *J. Mater. Chem. A.,* 2014, **2**, 2390-2396; (d) M. L. Sánchez, A. Primo and H. García, *Angew. Chem. Int. Ed.*, 2013, **52**, 11813 –11816.